Dendritic structural inhomogeneities in thin $Cs_{0.2}FA_{0.8}PbI_{2.93}Cl_{0.07}$ layers for perovskite solar cells

© M.S. Dunaevskiy[1,2], P.A. Alekseev[1,2], A.N. Smirnov[1], P.A. Gostishchev[3], D.O. Gren[3], A.D. Furasova[2], D.S. Saranin[2,3], E.I. Terukov[1,2]

[1] Ioffe Institute,
194021 St. Petersburg, Russia
[2] ITMO University (Physics and Engineering Mega-Faculty),
197101 St. Petersburg, Russia
[3] MISIS University,
119049 Moscow, Russia

E-mail: Mike.Dunaeffsky@mail.ioffe.ru

Received November 20, 2024
Revised December 4, 2024
Accepted December 4, 2024

In this work, the Kelvin probe microscopy (KPM) study of thin films $Cs_{0.2}(CH(NH_2)_2)_{0.8}PbI_{2.93}Cl_{0.07}$ (0.5 μm) with a frontal passivation coating of Al_2O_3 (10 nm) was performed. When using liquid-phase growth methods of $Cs_{0.2}(CH(NH_2)_2)_{0.8}PbI_{2.93}Cl_{0.07}$, the surface morphology is characterized by the presence of shagreen and surface profile fluctuations in the range of tens of nanometers due to the presence of stresses in the crystal lattice. Dendritic structural inhomogeneities with lateral dimensions of 10 μm and occupying about 25% of the surface were detected. A comprehensive KPM analysis allowed us to determine that the composition of the dendrites corresponds to δ-$CsPbI_3$. This indicates phase segregation in multicationic films with a non-passivated frontal surface. It is shown that in the absence of the upper protective layer, the initial $Cs_{0.2}(CH(NH_2)_2)_{0.8}PbI_{2.93}Cl_{0.07}$ film is transformed into dendritic regions of δ-$CsPbI_3$ and surrounding regions of $FAPbI_{2.93}Cl_{0.07}$. In the presence of the front passivation layer of Al_2O_3, the $Cs_{0.2}(CH(NH_2)_2)_{0.8}PbI_{2.93}Cl_{0.07}$ film is stable. The photopotential of the films and dendritic inhomogeneities under illumination was studied. It was found that under illumination with diffused sunlight, the dendritic structures are charged with a negative charge and a residual potential of $U_{res} = -100$ mV arises. When the illumination is turned off, a small residual potential arises at the boundaries of the dendritic structures, which weakens with a characteristic time of 20–30 minutes.

Keywords: Thin perovskite films, Scanning probe microscopy, Kelvin probe microscopy, structural inhomogeneity of thin films.

DOI: 10.61011/SC.2024.11.59958.7334

1. Introduction

The use of hybrid halide perovskites (HHP) of mixed cationic compositions $APbI_3$ (where A is an organic cation CH_3NH_3 (MA), $CH(NH_2)_2$ or Cs) is a common approach in photovoltaics to ensure high efficiency of solar cells (> 20%) and relevant stability under the influence of external factors (high-intensity light, elevated temperatures, oxygen, water vapor) [1]. The choice of the cationic composition of the HHP allows tuning the band gap (from 1.1 to 2.3 eV) [2]. According to the current state of development of the field, high efficiencies of solar cells (20–25%) based on HHP are achieved using photoactive layers with a crystalline lattice (CL) of $FAPbI_3$ [3]. However, the photoactive cubic phase α-$FAPbI_3$ has a tendency to spontaneous phase transition to the non-photoactive hexagonal polymorph (δ-$FAPbI_3$) [4] at room temperature, which is obviously within the operating range of solar cells (SCs). For stabilization of α-$FAPbI_3$ an approach based on cationic substitution of organic cation by Cs [5] is effective. Partial cationic substitution makes it possible to decrease the unit cell size and increase the energy barrier for the transition from the α-phase into the β-phase making α-phase kinetically more stable. The use of mixed $CsFAPbI_3$ compositions allows achieving high stability indices in $p-i-n$-solar cell architectures (more than 2000 h at constant photosaturation and 65°C temperature) [6]. A specific feature of thin films of HHP based on $CsFAPbI_3$ is the surface morphology in the form of shagreen, which is characterized by the appearance of surface dendrites. This feature is a result of stresses in the microcrystalline film during liquid-phase crystallization. The appearance of shagreen, as a consequence of stress relaxation in the film, can have a significant effect on the surface properties of $CsFAPbI_3$. In addition, the effect of an oxidizing external environment and cyclic thermal loads can initiate the process of phase segregation, accompanied by the formation of $CsPbI_3$ clusters at the grain boundaries of microcrystalline films [7]. The surface of perovskite layers is an area with an increased concentration of defects and a disrupted crystal structure. The accumulation of point defects (vacancies, interstitial atoms) in the bulk of the material leads to local distortions of the crystal lattice. This creates energetically favorable conditions for the onset of the phase transition from the

α-phase into the β-phase, and the surface states can serve as nucleation centers [8].

One of the standard approaches to passivation of the semiconductor surface for photovoltaic applications is the use of dielectric interlayers [9]. The use of nanocrystalline layers Al_2O_3 [10], SiO_2 [11] etc. provides compensation of surface states, reduces the rate of nonradiative recombination and suppresses possible electrochemical oxidation processes. Usually, the technological processes of deposition of dielectric interlayers are carried out using plasma methods [12] or atomic layer deposition (ALD) [13]. However, these methods are not applicable to microcrystalline layers based on HHP, since metal-organic compounds do not withstand the effects of high-energy particles and are soluble in typical ALD precursors. Ion beam deposition (IBD) is a promising alternative [14]. The IBD principle involves focusing a plasma beam on a target and deposition in a flow of scattered particles on a substrate. In this method, the plasma generation process is isolated from interaction with the substrate, but allows one to control the stoichiometry of the deposited dielectrics (introduction of gas — oxidizer), as well as the dynamics of deposition (plasma beam energy from 700 to 5000 eV [14], working gas flow). The high perfection of the structure of semiconductor layers obtained by ILN is reported, as well as the successful testing of the application of an oxide material — indium tin oxide (ITO) ($In_2O_3:SnO_2$) as a back electrode of semitransparent perovskite solar cells (SCs) [15].

This study focuses on the analysis of the specific features of phase segregation in thin-film $Cs_{0.2}(FA)_{0.8}PbI_{2.93}Cl_{0.07}$ with dendritic surface morphology, as well as the possibility to suppress this effect when applying passivation oxide materials by the PLD method. The Kelvin probe microscopy (KPM) method was used to study the surface potential of perovskite films „in the dark“ and „under illumination“ to determine the spatial inhomogeneity of photovoltage. In addition, the KPM method was used to study the processes of charge redistribution between structural inhomogeneities in the samples.

2. Specimens and methods of study

2.1. Materials

The following precursors were used to obtain perovskite films: i) formamidinium iodide (FAI, $> 99.99\%$) was purchased from Greatcell Solar (Australia), ii) lead iodide (PbI_2, $> 99.9\%$) and iii) cesium iodide (CsI, $> 99.99\%$) from „Lankhit LLC“ (Russia). Anhydrous organic solvents dimethylformamide (DMF) and dimethyl sulfoxide were purchased from Sigma-Aldrich and used as received without further purification. Ethyl acetate (EAC) was purchased from HPS (Russia).

2.2. Substrates

Perovskite films were fabricated on glass coated with $In_2O_3:SnO_2$ (ITO) ($R < 7\,\Omega$) by Zhuhai Kaivo (China).

2.3. Preparation of precursors

To prepare the perovskite solution, halide salts (CsCl, CsI, FAI, PbI_2) were used in molar ratios of $0.07:0.13:0.2:1$. The resulting mixture was dissolved in DMF:DMSO (volume ratio $4:1$) with a concentration of 1.35 M and stirred at a temperature of 50°C during 1 h.

2.4. Layer application and research

First, the ITO substrates were cleaned successively with detergents, deionized water, acetone and isopropyl alcohol (IPA) in an ultrasonic bath. Then, the substrates were activated under a UV-ozone cleaner for 30 min. The $CsFAPbI_3$ film was crystallized on top of the ITO by the antisolvent method. The deposition process of the perovskite layers was carried out in a glove box with an inert nitrogen atmosphere. The perovskite solution was deposited on the substrate fixed on a centrifuge, which rotated according to the following program: 1 s — 1000 rpm, 4 s — 3000 rpm/30 s — 5000 rpm. 400 μl EAC was dropped onto the substrate at 20th s after the start of the first rotation step. The substrates were then annealed at 70°C (1 min) and 105°C (30 min) to form the corresponding perovskite phase.

Both samples without a protective top coating and samples with a protective coating SnO_2 and Al_2O_3 were studied. Deposition of $Cs_{0.2}(FA)_{0.8}PbI_3Cl_{0.07}$ layers was performed by the liquid-phase spin-coating method with crystallization in an antisolvent [16]. Deposition of SnO_2 and Al_2O_3 layers was performed by the ion-beam sputtering method on a NIKA-130500 setup (manufactured by OOO LVT+, RF). The setup chamber was evacuated to a base pressure of $2 \cdot 10^{-2}$ Pa. To obtain oxide coatings, metal targets (Al, Sn) of purity $4N$ (manufactured by OOO Girmet, Russian Federation) were used. The working gas of the ion source was Ar (purity 99.998%), the oxidizer gas was — O_2 (99.999%). Before the PLD process, the target was plasma cleaned for 10 min. The parameters of the application processes were as follows: source voltage 1000 V, source current 100 mA, O_2 — 0.5 l/h. The deposition rate (determined empirically) is 0.6 nm/min for Al_2O_3, 1.1 nm/min for SnO_2. During the oxide coating processes, the target and substrates for deposition were thermostatted in the temperature range from 25 to 35° with water cooling. The multilayer structures were not annealed or post-treated before the KPM study.

To study the structural and photovoltaic properties of $Cs_{0.2}(FA)_{0.8}PbI_3Cl_{0.07}$ scanning probe microscopes NTegra-Aura (NTMDT, Russia) and metallized NSG10/Pt probes NSG10/Pt (TipsNano, Russia) with $R = 30$ nm probe point radius were used. The scanning probe microscope (SPM)

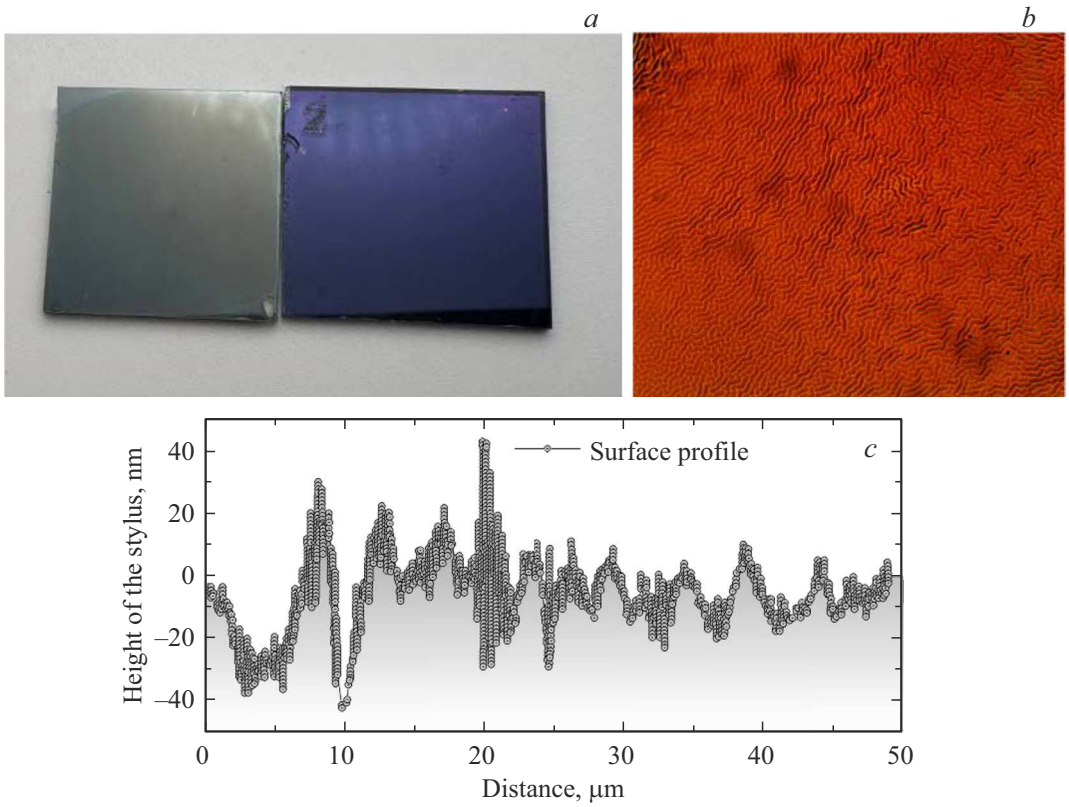

Figure 1. *a* — photos supporting configurations sample $Cs_{0.2}(FA)_{0.8}PbI_3Cl_{0.07}$ (left) and with coating Al_2O_3 (right); *b* — film surface snapshot $Cs_{0.2}(FA)_{0.8}PbI_3Cl_{0.07}$ at increase of $\times 100$; *c* — surface profile $Cs_{0.2}(FA)_{0.8}PbI_3Cl_{0.07}$, measured by method stylus profilometry.

laser recording probe oscillations emitted at a wavelength of $1.3\,\mu$m, and the radiation was not absorbed by the layer under study. The surface was illuminated in two ways: with a LED lamp with an emission spectrum of ($\lambda_{exc} = 400-700$ nm) and by scattered sunlight. To determine the photovoltage, a two-pass mode of Kelvin-probe microscopy was used. In the first pass, the surface relief was measured in the semi-contact mode, while the oscillation amplitude was 20–30 nm. In the second pass, the probe scanned the surface, moving at a constant probe-surface distance of 20 nm, while the amplitude of oscillations caused by a periodic change in the probe-sample potential was measured (with its subsequent zeroing). The amplitude of the applied alternating voltage was $U_{ac} = 1$ V. The frequency of the alternating signal was selected close to the value of the mechanical resonance of the cantilever (in the range from 100 to 300 kHz). Measuring the surface relief allowed us to estimate the degree of granularity, characteristic grain sizes and characteristic roughness of perovskite films. It should be noted that the grain sizes and the presence of grain boundaries can significantly affect the efficiency of photovoltaic conversion of perovskite SCs. Measuring the KPM potential „in the dark“ and „under illumination“ allowed us to determine the photovoltaic force of the films under study. Raman spectra (Raman spectroscopy) were measured at room temperature in backscatter geometry using a Horiba LabRAM HREvo UV-VIS-NIROpen [17] spectrometer.

3. Experimental results

The studied samples were $Cs_{0.2}(FA)_{0.8}PbI_3Cl_{0.07}$ 500 nm thick layers of deposited on a 220 nm thick layer of ITO, which was deposited on a glass substrate (Figure 1, *a*). A photographic image of $Cs_{0.2}(FA)_{0.8}PbI_3Cl_{0.07}$ samples, as well as the dendritic surface morphology (optical microscopy, magnification $\times 20$) are shown in Figure 1, *b*. Nanocrystalline dielectric, as well as Al_2O_3 — SnO_2 — a wide-gap *n*-type conductivity material, which is used in *p–i–n* SCs in the electron-transport layer, were used as passivation interlayers.

The KPM method was used to study (Figure 2) thin perovskite films $Cs_{0.2}FA_{0.8}PbI_{2.93}Cl_{0.07}$ with a protective coating Al_2O_3 and films without a protective coating.

It was found that in both cases the samples were granular films with a characteristic lateral grain size of 150–200 nm. An important difference between the samples is the presence of dendritic structural inhomogeneities in the samples without the top protective coating (see Figure 2, *b* and *d*). The characteristic lateral size of the dendritic structures is ~ 10 microns. The fraction of the surface occupied by the dendritic structures was calculated in the Gwyddion

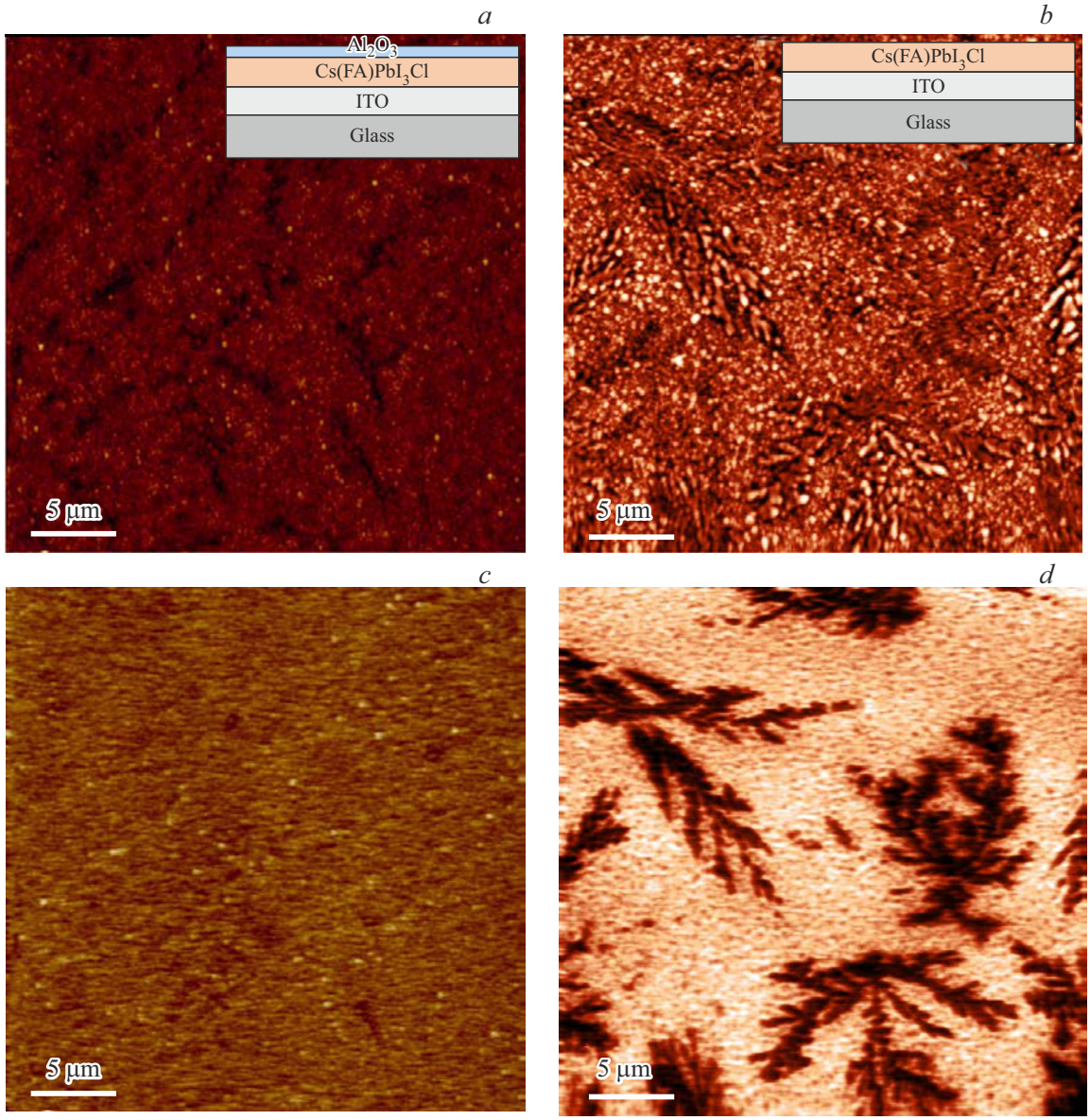

Figure 2. *a* — topography ($30 \times 30\,\mu$m) and *c* — KPM on sample $Cs_{0.2}(FA)_{0.8}PbI_3Cl_{0.07}$ (with protective coating Al_2O_3); *b* — topography ($30 \times 30\,\mu$m) and *d* — KPM on sample $Cs_{0.2}(FA)_{0.8}PbI_3Cl_{0.07}$ (without protective coating).

program [18] and was $\sim 25\%$. The size of the minimal branches of the dendritic structures is comparable with the characteristic grain size (~ 200 nm). It should be noted that the Kelvin potential measurement in Figure 2, *d* was carried out when illuminated, and it can be seen that the dendritic structures have a residual negative potential of $U_{\text{light}} = -100$ mV (relative to the surrounding layer). After the measurements under illumination (Figure 3, *a*), the surface potential measurements were also performed „in the dark" after 10 min and after 30 min (see Figure 3, *b* and *c*).

It can be seen that in transition „to darkness" a small residual potential $U_{\text{dark}} = +30$ mV appears on the dendritic structures, which then weakens over time to zero with a characteristic time of 20–30 min. It is especially worth noting that the sign of the residual potential on the dendritic structures „in darkness" is opposite to the potential „when illuminated". Micro-Raman measurements were performed on the dendritic structures and on the main part of the layer $Cs_{0.2}FA_{0.8}PbI_{2.93}Cl_{0.07}$. The measured Raman peak positions on the dendritic structures (55 and 110 cm^{-1}) indicate that they consist mainly of δ-$CsPbI_3$ and CsI [19]. In the initial films, the amount of Cs was 20% (compared to 80% for FA). Since the fraction of the layer occupied by dendrites, according to atomic force microscopy (AFM), is $\sim 25\%$, it can be assumed that the chemical composition of the bulk of the dendrites — is δ-$CsPbI_3$, and the grain boundaries are likely to contain CsI. The bulk of the surrounding layer (75%) apparently consists of $FaPbI_3$. Namely, the initial film $Cs_{0.2}FA_{0.8}PbI_{2.93}Cl_{0.07}$ without the upper protective

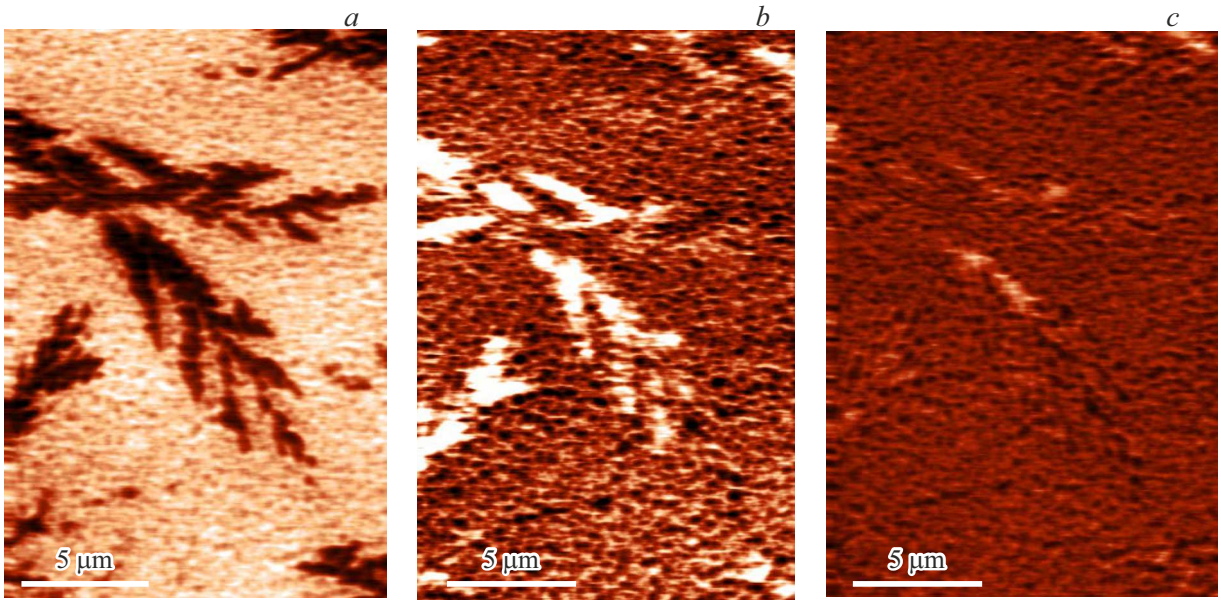

Figure 3. Measurements of ($15 \times 22\,\mu$m) potential using sample $Cs_{0.2}(FA)_{0.8}PbI_3Cl_{0.07}$ (without protective coating); *a* — KZM „when illuminated“; *b* — KZM „in darkness“ in 10 min; *c* — KZM „in darkness“ in 30 min.

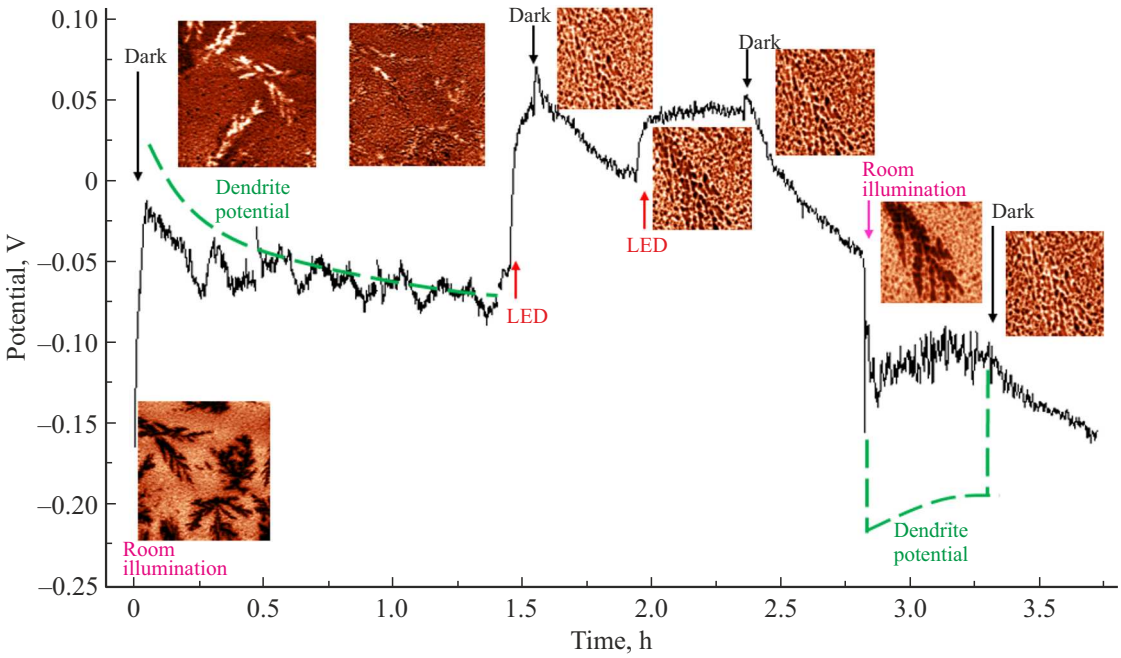

Figure 4. $Cs_{0.2}FA_{0.8}PbI_{2.93}Cl_{0.07}$ layer potential dependence under illumination and „in darkness“. The green dotted line shows the potential on dendritic structures. The inserts show characteristic KPM images of the potential on the layer $Cs_{0.2}FA_{0.8}PbI_{2.93}Cl_{0.07}$. (A color version of the figure is provided in the online version of the paper).

layer disintegrates into δ-$CsPbI_3$ (dendrites) and the surrounding $FAPbI_3$.

Measurements of the KPM potential „under illumination“ and „in the dark“ were also performed on the main (non-dendritic) part of the $Cs_{0.2}FA_{0.8}PbI_{2.93}Cl_{0.07}$ films. When the surface is illuminated „by room light“ the photo-emf sign — is negative and is about -100 – -200 mV. Then, upon transition „to darkness“ the potential returns to its initial value (see Figure 4). In similar experiments, but under illumination by an LED lamp with an emission spectrum of $\lambda_{exc} = 400-700$ nm, the sign of the photo-emf — is positive and amounts to 30–70 mV, which is apparently due to the narrower irradiation spectrum.

The dynamics of surface potential changes strongly depends on photoinjection processes (presence of exposure and dark conditions). When passing from photosaturation

conditions to dark conditions, a sharp increase in the surface potential is observed in the range of several minutes. In this case, repeated switching on of the light source makes this indicator gradually decrease. In case of exposure, electron-hole pairs are generated in the perovskite film. Free carriers increase the conductivity and change the local electric field on the surface, which results in the decrease of the surface potential. The availability of minor photocarriers leads to interaction with ionic defects (vacancies, interstices, antistructures), which causes their redistribution in the lattice [20,21]. When passing to dark conditions the surface potential increases due to a decrease in the number of free charge carriers and restoration of the original band bending. The ions return to equilibrium positions as the electric fields relax. Thus, it can be concluded that phase segregation accompanied by the formation of dendritic regions on the surface leads to the appearance of uncompensated defect centers. The analysis of the nature of defect centers, carried out by our group in the previous work [22], shows that the most characteristic influence for the composition of $Cs_{0.2}FA_{0.8}PbI_{2.93}Cl_{0.07}$ is that of the defects — vacancies of the formamidine and iodine cations, which have acceptor and donor specificity, respectively. The observed dynamics of changes in the surface potential in this research work directly indicates the metastability of the frontal interface states and the need for passivation.

4. Conclusion

It is shown that in the $Cs_{0.2}FA_{0.8}PbI_{2.93}Cl_{0.07}$ samples without the upper protective layer, the dendritic structures are formed occupying$\sim$ 25% of the layer. The characteristic lateral sizes of the dendritic structures are $10\,\mu$m. The size of the minimal branches of the dendritic structures is comparable with the characteristic grain size (~ 200 nm) in the films. It is shown that the composition of the dendrites is δ-$CsPbI_3$. It is shown that if the upper protective layer is unavailable, the initial $Cs_{0.2}FA_{0.8}PbI_{2.93}Cl_{0.07}$ film disintegrates into dendritic regions δ-$CsPbI_3$and surrounding regions $FAPbI_3$. If the upper protective layer is available, the film $Cs_{0.2}FA_{0.8}PbI_{2.93}Cl_{0.07}$ is stable. The photovoltaic properties of the dendritic structures differ from the properties of the main part of the $Cs_{0.2}FA_{0.8}PbI_{2.93}Cl_{0.07}$ films. When illuminated, an additional negative charge accumulates on the dendritic structures, creating a potential of $U_{\text{light}} = -100$ mV. When passing to darkness, a slow discharge of dendritic structures occurs (on the time scale 20$-$30 min). $Cs_{0.2}FA_{0.8}PbI_{2.93}Cl_{0.07}$ samples with the upper protective layer are quite homogeneous and do not contain any dendritic structures. It can be assumed that the presence of dendritic structures is a sign of degradation of the perovskite films $Cs_{0.2}FA_{0.8}PbI_{2.93}Cl_{0.07}$ and it is necessary to take measures to prevent their occurrence.

Funding

This study was supported by grant No. 24-62-00022 from the Russian Science Foundation, https://rscf.ru/project/24-62-00022/

Conflict of interest

The authors declare that they have no conflict of interest.

References

[1] NREL efficiency chart 2024, https://www.nrel.gov/pv/cell-efficiency.html/
[2] B. Chen, P.N. Rudd, S. Yang, Y. Yuan, J. Huang. Chem Soc. Rev., **48**, 3842 (2019).
[3] S.A. Kulkarni, T. Baikie, P.P. Boix, N. Yantara, N. Mathews. J. Mater. Chem. A: Mater., **2**, 9221 (2014).
[4] D.T. Cuzzupé, F. Ünlü, K. Lě, R. Bernhardt, M. Wilhelm. Sci. Rep., **12**, 10241 (2022).
[5] Z. Huang, Y. Bai, X. Huang, J. Li, Y. Wu, Y. Chen, K. Li, X. Niu, N. Li, G. Liu, Y. Zhang, H. Zai. Nature, **623**, 531 (2023).
[6] V.L. Pool, B. Dou, D.G. Van Campen. Nature Commun., **8**, 14075 (2017).
[7] M. Lyu, N.G. Park. Solar RRL, **4**, 2000331 (2020).
[8] M.P.U. Haris, S. Kazim, S. Ahmad. ACS Appl Energy Mater., **14**, 24546 (2021).
[9] A. Yakusheva, D. Saranin, D. Muratov, P. Gostishchev. Small, **18**, 2201730 (2022).
[10] J. Yang, Y. Chen, W. Tang, S. Wang, Q. Ma, Y. Wu. J. Energy Chem., **48**, 217 (2020).
[11] P. Gostishchev, D. Saranin, L. Luchnikov, D. Muratov. Solar RRL, **7**, 2200941 (2023).
[12] J. Xu, C.C. Boyd, Z.J. Yu, A.F. Palmstrom, D.J. Witter, B.W. Larson, R.M. France, J. Werner. Science, **367**, 1097 (2020).
[13] J.S. Yun, J. Kim, T. Young, R.J. Patterson. Adv. Funct. Mater., **28**, 1705363 (2018).
[14] N.A. Manshor, Q. Wali, K.K. Wong, S.K. Muzakir, A. Fakharuddin, L. Schmidt-Mende, R. Jose. Phys. Chem. Chem. Phys., **18**, 21629 (2016).
[15] E.J. Juarez-Perez, L.K. Ono, M. Maeda, Y. Jiang. J. Mater. Chem. A, **6**, 9604 (2018).
[16] Q. Wali, Y. Iqbal, B. Pal, A. Lowe, R. Jose. Solar Energy Mater. Solar Cells, **179**, 102 (2018).
[17] D.Yu. Usachov, V.Yu. Davydov, V.S. Levitskii. ACS Nano, **11**, 6336 (2017).
[18] D. Necas, P. Klapetek. Cent. Eur. J. Phys., **10**, 181 (2012).
[19] F. Ke, C. Wang, C. Jia, N.R. Wolf, J. Yan, S. Niu, T.P. Devereaux, H.I. Karunadasa, W.L. Mao, Y. Lin. Nature Commun., **12**, 461 (2021).
[20] T. Leijtens, E.T. Hoke, G. Grancini, D.J. Slotcavage, G.E. Eperon, J.M. Ball, M. De Bastiani. Adv. Energy Mater., **5**, 1500962 (2015).
[21] Y. Deng, Z. Xiao, J. Huang. Adv. Energy Mater., **5**, 1500721 (2015).
[22] A.A. Vasilev, D.S. Saranin, P.A. Gostishchev, S.I. Didenko, A.Y. Polyakov, A. Di Carlo. Optical Mater.: X, **16**, 100218 (2022).

Translated by J.Savelyeva